Materials Science and Engineering A 397 (2005) 288–296

www.elsevier.com/locate/msea

First-principles calculations and thermodynamic modeling of the Ni–Mo system

S.H. Zhou *, Y. Wang, C. Jiang, J.Z. Zhu, L.-Q. Chen, Z.-K. Liu

Department of Materials Science and Engineering, The Pennsylvania State University, University Park, PA 16802, USA

Received 17 December 2004; received in revised form 9 February 2005; accepted 9 February 2005

Abstract

The phase equilibria and thermodynamic properties of the Ni–Mo system were analyzed by combining a first-principles approach and calculation of phase diagram (CALPHAD) technique. The first-principles calculation results indicate that Ni_2Mo and Ni_8Mo are stable in addition to Ni_3Mo and Ni_4Mo, and δ-NiMo is not stable at 0 K, both in contradiction to the existing phase relationships in the Ni–Mo system. The enthalpies of the mixing of the bcc and fcc solid solution phases were also predicted by first-principles calculations using the special quasirandom structures. In the present work, the non-stoichiometric δ-NiMo and Ni_3Mo phases were modeled using three- and two-sublattice models, respectively. The Ni_2Mo, Ni_4Mo and Ni_8Mo phases were treated as stoichiometric compounds. Based on the first-principles data from the present work and experimental data in the literature, the Gibbs energy functions of individual phases were evaluated, and a new Ni–Mo phase diagram was presented.
© 2005 Elsevier B.V. All rights reserved.

Keywords: Mo–Ni; phase diagram; Thermodynamic modeling; First-principles calculation

1. Introduction

The performance of Ni-base superalloys depends on its ability to withstand high temperatures without failure. A tremendous amount of research has been devoted to improving their performance at higher temperatures and for longer periods of time [1–7]. Understanding of alloying effects on phase stability is critical in providing quantitative guidelines for alloy development and processing design. The present work focuses on the thermodynamic study of the Ni–Mo system through first-principles calculations and CALPHAD modeling.

Thermodynamic modeling of the Ni–Mo system was first carried out by Frisk [8] in which six phases were considered. The liquid, fcc and bcc phases were treated with the one-sublattice model, the δ-NiMo phase with three-sublattice model as $(Ni)_{24}(Mo, Ni)_{20}(Mo)_{12}$, and the Ni_3Mo and Ni_4Mo phases as two-sublattice stoichiometric compounds. Based on Frisk's work [8], Cui et al. [9] modified the thermodynamic description of the Ni–Mo system by modeling the Ni_3Mo phase with a two-sublattice model, $(Mo, Ni)_3(Mo, Ni)_1$, to account for its homogeneity range. The calculated phase diagram by Cui et al. [9] revealed unrealistic behavior of the δ-NiMo phase at low temperature as shown in Fig. 1. The Ni–Mo system was also studied by Morishita et al. [10] in the Ni–Mo–B ternary system to design a new $NiMo_2B_2$-dispersed Ni-based alloy. In their work, the Gibbs energy functions of liquid, fcc and δ-NiMo (as a stoichiometric compound) in the Ni–Mo system were evaluated, while other compounds were not considered in their work.

In addition to the three intermetallic phases considered by Frisk [8] and Cui et al. [9], literature data indicated the possible existence of Ni_2Mo [11] and Ni_8Mo [12]. To investigate the stability of the compounds in the Ni–Mo system, Wang et al. [13] calculated their enthalpies of formation using VASP [14]. Furthermore, the recent development in the first-principles calculations enables us to calculate the enthalpy of mixing in fcc and bcc using the special quasirandom structures (SQS) [15,16], which mimic the random mixing in fcc

* Corresponding author. Present address: Metals and Ceramics Sciences Program, Ames Laboratory, Department of Energy, 116 Wilhelm, Ames, IA 50011, USA. Tel.: +1 515 294 5489; fax: +1 515 294 4291.
E-mail address: szhou@ameslab.gov (S.H. Zhou).

0921-5093/$ – see front matter © 2005 Elsevier B.V. All rights reserved.
doi:10.1016/j.msea.2005.02.037

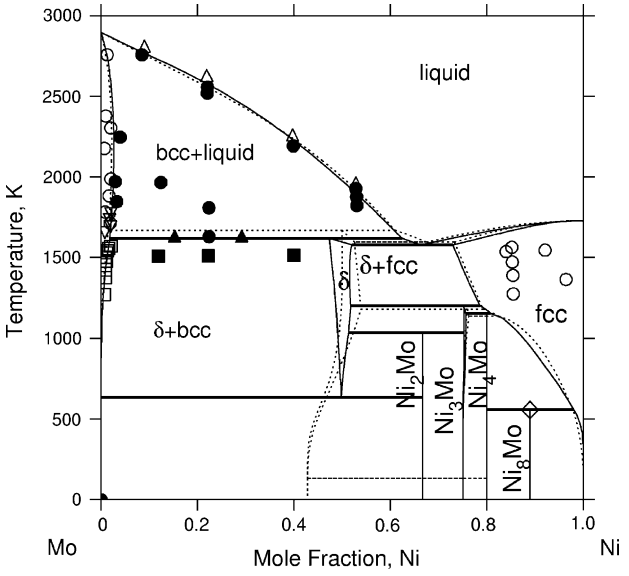

Fig. 1. The phase diagram calculated using the parameters of Ni_3Mo (three-sublattice model) with the experimental data (◊) three-phase equilibrium [12]; (▲) three-phase equilibrium [17]; (◯) single phase field, (△) liquid phase field, (●) two-phase field with liquid phase, (■) two-phase field [18]; (□) phase boundary [19] and (▽) bcc phase boundary [20]; The dotted-lines calculated phase diagram using the parameters by Cui et al. [9].

and bcc using relative small supercells. These data are used to guide the evaluation of thermodynamic parameters.

Based on the newly obtained enthalpy of formation of compounds by first-principles calculations [13], the enthalpy of mixing in fcc and bcc by SQS in the present work, and experimental data in the literature, the thermodynamic modeling of the Ni–Mo system was carried out, and a new Ni–Mo phase diagram was predicted. In this paper, the experimental information in the literature and first-principles calculations will be reviewed first, followed by thermodynamic modeling and discussions.

2. Experimental information and first-principles calculations

In thermodynamic modeling, the Gibbs energy functions of individual phases are modeled with respect to temperature, pressure and composition. Models are based on crystal structures of phases, and model parameters are evaluated from the phase equilibrium and thermochemical data. The crystal structure information of the Ni–Mo system is shown in Table 1, and phase equilibrium and thermochemical data are reviewed in this section.

2.1. Experimental information

The experimental data in the literature, reviewed in detail by Frisk [8] and Cui et al. [9], are briefly presented here.

The three-phase equilibria in Ni–Mo were measured by Grube and Schlecht [17] using the thermal analysis method.

Table 1
Intermetallic compounds in the Ni–Mo system

Phases	Prototype	Structure-bericht	Space group	Ref.
δ-NiMo	NiMo	–	$P2_12_12_1$	[18,33,34]
Ni_2Mo	Pt_2Mo	–	*Immm*	[38]
Ni_3Mo	Cu_3Ti	$D0_a$	*pmmn*	[18]
Ni_4Mo	Ni_4Mo	$D1_a$	*I*4/*m*	[18]
Ni_8Mo	Pt_8Ti	–	4/*m*2/*m*2/*m*	[12]

They also studied the liquid + fcc two-phase equilibrium in the composition range of 70–85 at.% Ni. The liquidus boundary was determined by Casselton and Hume-Rothery [18] using the thermal analysis, metallurgraphic, and X-ray diffraction methods. They also investigated the equilibria among bcc, fcc, δ-NiMo, Ni_3Mo and Ni_4Mo. The phase equilibria at temperatures below 1600 K were investigated by Heijwegen and Rieck [19] by means of the diffusion couple technique and electron probe microanalysis (EPMA). The solidus boundary of bcc was investigated by Kang et al. [20] through the powder sintering technique and the electrolytic phase separation method and using EPMA.

The compound Ni_2Mo was found by Pearson et al. [11] in a 76Ni–13Al–9Mo–2Ta alloy aged at 1033 K using an electron microscope, while Heijwegen and Rieck [19] did not find it in binary diffusion couple samples treated between 1073 and 1550 K. Thus the decomposition temperature of Ni_2Mo seems between 1033 and 1073 K. The stability of the compound Ni_8Mo was investigated by Mayer and Urban [12] using a high-voltage electron microscope. The decomposition temperature was found to be 555 ± 10 K.

The enthalpy of formation of δ-NiMo was measured by Spencer and Putland [21] and Kubaschewski and Hoster [22] using a high-temperature adiabatic calorimeter. The activity data in fcc and Gibbs energy of mixing of fcc were measured by various authors [23–27] using electromotive force (EMF) method. The activities of Mo in fcc measured by Meshkov et al. [24] at 1273 K are compatible with those by Tsai [25] at 1250 K, and slightly different from those by Katayama et al. [23] at 1223 K and Pejryd [26] at 1273 K. The data by Koyama et al. [27] show a very strong temperature-dependency of Gibbs energy of mixing in fcc which results in a positive Gibbs energy of mixing in $Ni_{0.775}Mo_{0.225}$ fcc when extrapolated to room temperature (see Fig. 2).

2.2. First-principles calculations

The total energy of fcc-Ni and bcc-Mo and all binary compounds were calculated by means of VASP [14] with Vanderbilt ultrasoft pseudopotential [28] and the generalized gradient approximation (GGA) [14] using the high precision choice. The 3d4s and 4d5s shells were treated as valence states with core radii of 2.43 and 2.75 a.u. for Ni and Mo, respectively. Monkhost $15 \times 15 \times 15$ *k* points were used for the pure elements Ni and Mo, $11 \times 11 \times 11$ *k* points for Ni_2Mo, Ni_3Mo, Ni_4Mo, and Ni_8Mo and $6 \times 6 \times 6$ *k* points for the following end-member of δ-NiMo: $Ni_{24}(Mo_{20})Mo_{12}$, $Ni_{24}(Ni_4$,

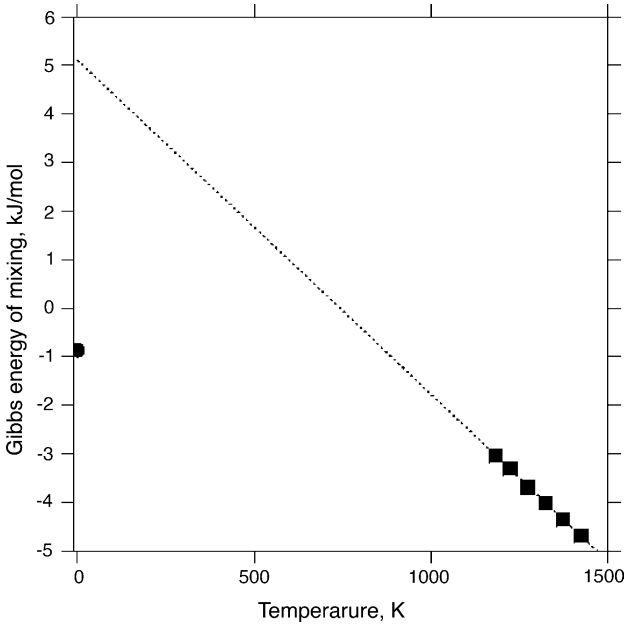

Fig. 2. The Gibbs energy of mixing of fcc extrapolated from the data (■) [27] at composition $Ni_{0.775}Mo_{0.225}$ with the corresponding first-principles data (●).

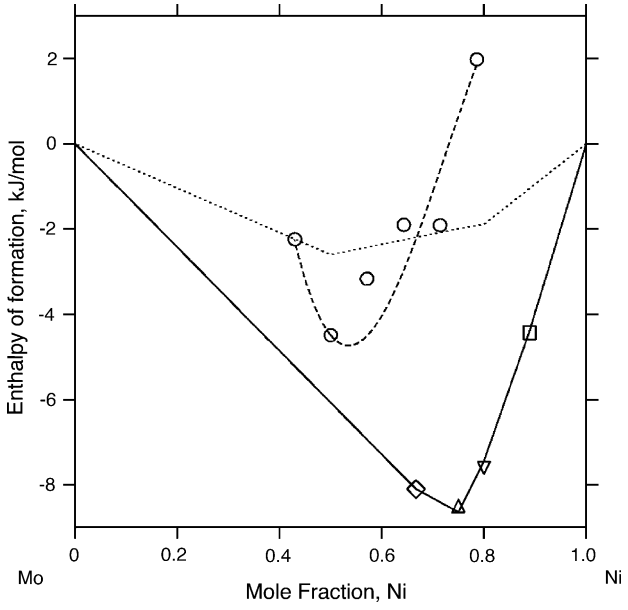

Fig. 3. The calculated enthalpy of formation (—) of the binary Ni–Mo system and enthalpy of mixing (- - -) of the compound δ-NiMo at 0 K with the first-principles calculation results [13] of (◯) δ-NiMo, (◇) Ni_2Mo, (△) Ni_3Mo, (▽) Ni_4Mo, and (□) Ni_8Mo and the dotted-line (···) calculated using the parameters by Cui et al. [9]. Reference state: fcc-Ni and bcc-Mo.

$Mo_{16})Mo_{12}$, $Ni_{24}(Ni_{16}, Mo_4)Mo_{12}$, and $Ni_{24}(Ni_{20})Mo_{12}$ [13]. To ensure that the unit cell of unstable end-member still corresponds to stable structure, we only relaxed the cell volume of the unstable end-member without local lattice relaxations due to the structure instability [29].

The enthalpy of formation of a compound Φ, ΔH_f^{Φ}, is calculated by subtracting the total energy of fcc-Ni and bcc-Mo, $E_{TOT}^{fcc\text{-}Ni}$ and $E_{TOT}^{bcc\text{-}Mo}$, from the total energy of the compound Φ, E_{TOT}^{Φ}

$$\Delta H_f^{\Phi} = E_{TOT}^{\Phi} - x_{Ni}^{\Phi} E_{TOT}^{fcc\text{-}Ni} - x_{Mo}^{\Phi} E_{TOT}^{bcc\text{-}Mo} \quad (1)$$

where x_i^{Φ} is the mole fraction of component i in Φ. The calculated enthalpies of formation are plotted in Fig. 3 and listed in Table 2.

Due to the lack of experiments, the isostructure enthalpies of mixing of the bcc and fcc solid solution phases were calculated in the present study using 16-atom SQS's [15,16] for the compositions $x_{Ni} = 0.25$, 0.5 and 0.75, respectively. The derivations of the SQS's used in the present calculations were discussed in details in the literature [16]. The energetics of the SQS's as well as bcc-Ni and fcc-Mo were calculated using the GGA pseudopotentials within VASP. Spin-polarized calculations were performed to account for the ferromagnetic nature of Ni. The first-principles data shows that energy difference, $\Delta G^{bcc \to fcc}$ ($\Delta G^{bcc \to fcc} = G^{fcc} - G^{bcc}$), of element Mo is 39.51 kJ/mol, while $\Delta G^{bcc \to fcc}$ calculated by the CALPHAD approach using pure element database by Dinsdale [30] is 15.20 kJ/mol. This discrepancy is due to the instability of fcc-Mo as discussed in the literature [29]. Using the same arguments as that of the unstable end-members of the compounds, we only relaxed the cell volume of the SQS's without local lattice relaxations due to the structure instability of fcc-Mo and bcc-Ni [29]. The calculated total energies of the SQS's in both fcc and bcc structures at compositions $Ni_{0.75}Mo_{0.25}$, $Ni_{0.5}Mo_{0.5}$ and $Ni_{0.25}Mo_{0.75}$ are given in Table 2 together with the derived isostructure enthalpies of mixing of bcc and fcc plotted in Fig. 4. The enthalpies of mixing in Table 2 were used in the thermodynamic modeling.

In Fig. 3, the first-principles calculated enthalpy of formation of the δ-NiMo phase is above the solid-line between the pure bcc-Mo and Ni_2Mo phases. This indicates that δ-NiMo is not stable at 0 K. The dotted-line in Fig. 3 illustrates the enthalpy of formation calculated using the parameters by Cui et al. [9] at 298 K, which shows significant deviations from the present first-principles data.

3. Thermodynamic models

Thermodynamic models in the present work are based on the sublattice models developed by Sundman and Agren [31]. The number of sublattice and the number of sites per sublattice are constructed based on crystal structures of phases though combination of similar sublattices is often needed due to limited data available.

3.1. Liquid, fcc and bcc phases

Liquid, fcc and bcc were modeled as random solutions with the one-sublattice model (Mo, Ni). The Gibbs energy is

Table 2
First-principles calculation results

Phase	Prototype	Formula	eV/atom	ΔH (kJ/mol)	Ref.
Ni	fcc	Ni	−5.4827	0	[13]
Ni	bcc	Ni	−5.38605	9.33	This work
Mo	bcc	Mo	−10.8271	0	[13]
Mo	fcc	Mo	−10.4176	39.51	This work
$Ni_{0.25}Mo_{0.75}$	bcc-SQS16	$Ni_{0.25}Mo_{0.75}$	−9.3714	9.145	This work
$Ni_{0.50}Mo_{0.50}$		$Ni_{0.50}Mo_{0.50}$	−7.9977	10.45	This work
$Ni_{0.75}Mo_{0.25}$		$Ni_{0.75}Mo_{0.25}$	−6.6934	5.083	This work
$Ni_{0.25}Mo_{0.75}$	fcc-SQS16	$Ni_{0.25}Mo_{0.75}$	−9.2258	−4.063	This work
$Ni_{0.50}Mo_{0.50}$		$Ni_{0.50}Mo_{0.50}$	−8.0161	−6.405	This work
$Ni_{0.75}Mo_{0.25}$		$Ni_{0.75}Mo_{0.25}$	−6.7640	−4.663	This work
δ-NiMo	NiMo	$Ni_{24}(Mo_{20})Mo_{12}$	−8.5599	−2.24	This work
		Ni_{24} $(Ni_4Mo_{16})Mo_{12}$	−8.2014	−4.49	[13]
		$Ni_{24}(Ni_8Mo_{12})Mo_{12}$	−7.8022	−2.80	This work
		$Ni_{24}(Ni_{12}Mo_8)Mo_{12}$	−7.4006	−0.89	This work
		$Ni_{24}(Ni_{16}Mo_4)Mo_{12}$	−7.0108	−0.10	This work
		$Ni_{24}(Ni_{20})Mo_{12}$	−6.6073	1.98	This work
Ni_2Mo	Pt_2Mo	Ni_2Mo	−7.3507	−8.34	[13]
Ni_3Mo	Cu_3Ti	Mo_3Mo	−10.385	42.65	This work
		Ni_3Mo	−6.9073	−8.54	[13]
		Mo_3Ni	−9.3141	17.06	This work
		Ni_3Ni	−5.4532	2.84	This work
Ni_4Mo	Ni_4Mo	Ni_4Mo	−6.6298	−7.55	[13]
Ni_8Mo	Pt_8Ti	Ni_8Mo	−6.1225	−4.44	[13]

expressed as

$$G_{\mathrm{m}}^{\Phi} = \sum_{i=\mathrm{Mo,Ni}} x_i^{\circ}G_i^{\Phi} + RT \sum_{i=\mathrm{Mo,Ni}} x_i \ln x_i + {}^{\mathrm{xs}}G_{\mathrm{m}}^{\Phi} \qquad (2)$$

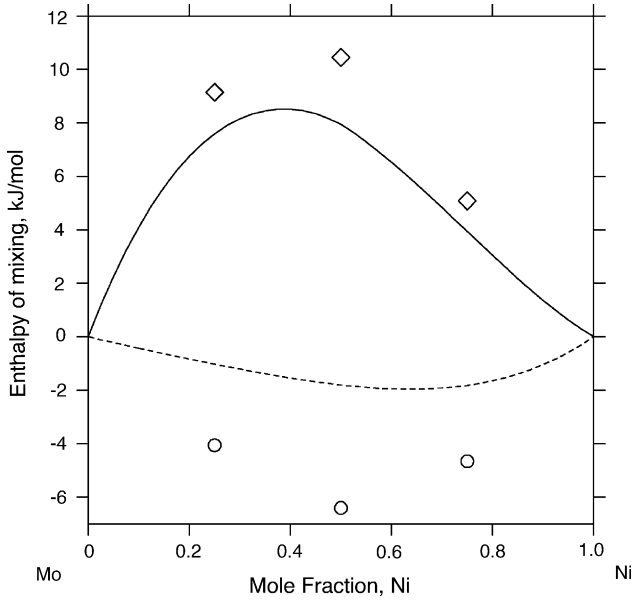

Fig. 4. The calculated isostructure enthalpy of mixing of bcc (—) referred to bcc-Ni and bcc-Mo and fcc (- - -) referred to fcc-Ni and fcc-Mo with the first-principles calculation data (◊) for bcc and (◯) for fcc.

where ${}^{\circ}G_i^{\Phi}$ (i = Mo, Ni) is the Gibbs energy of the pure element i with the structure Φ from the database by Dinsdale [30]. ${}^{\mathrm{xs}}G_{\mathrm{m}}^{\Phi}$ is the excess Gibbs energy, expressed in the Redlich–Kister polynomial [32],

$${}^{\mathrm{xs}}G_{\mathrm{m}}^{\Phi} = x_{\mathrm{Mo}}x_{\mathrm{Ni}} \sum_{j=0}^{n} {}^{j}L_{\mathrm{Mo,Ni}}^{\Phi}(x_{\mathrm{Mo}} - x_{\mathrm{Ni}})^j \qquad (3)$$

where ${}^{j}L_{\mathrm{Mo,Ni}}^{\Phi}$ is the jth interaction parameter between component Mo and Ni, expressed as ${}^{j}a^{\Phi} + {}^{j}b^{\Phi}T$, with ${}^{j}a^{\Phi}$ and ${}^{j}b^{\Phi}$ being model parameters to be evaluated.

3.2. δ-NiMo phase

δ-NiMo has the pseudo-tetragonal structure with space group $P2_12_12_1$ [13,33,34]. The unit cell of δ-NiMo has 56 atoms distributed in four sublattices, i.e. $(Ni)_{24}^{12}(Mo, Ni)_{20}^{14}(Mo)_8^{15}(Mo)_4^{16}$, where the superscript is the coordination number and the subscript is the number of the sites in the sublattice. According to the analysis by Andersson et al. [35], the sublattice with the coordination number of 12 is preferred by fcc elements, while sublattices with the coordination numbers of 14 and 15 are favorable for bcc elements. In this work, the reference state fcc was selected for the first sublattice and bcc for other sublattices. To simplify the description, the third and forth sublattices occupied by Mo only were combined, and the three-sublattice model, $(Ni)_{24}(Mo, Ni)_{20}(Mo)_{12}$ was used, the same as in Refs. [8,9],

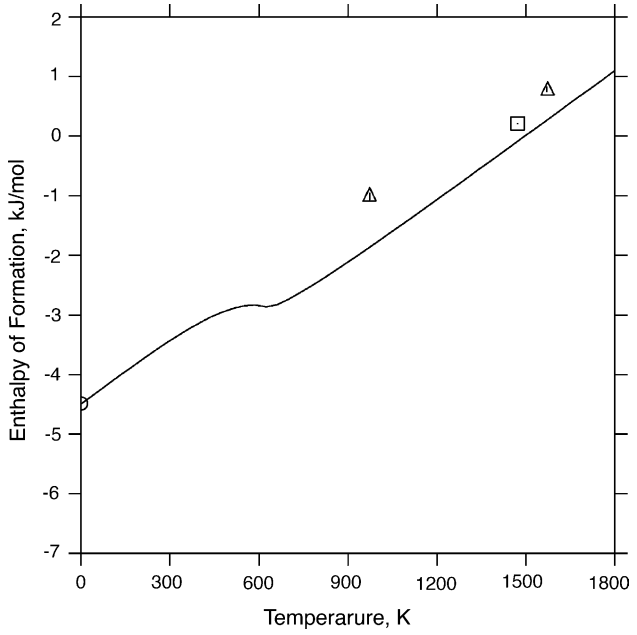

Fig. 5. The calculated enthalpy of formation of δ-NiMo ($x_{Ni} = 0.5$) in comparison with the first-principles calculation data (◯) and the experimental data (△) [21] and (□) [22]. Reference state: fcc-Ni and bcc-Mo.

and its Gibbs energy is given as:

$$G_m^{\delta} = \sum_{i=\mathrm{Mo,Ni}} y_i^{\mathrm{II}\circ} G^{\delta}_{\mathrm{Ni}:i:\mathrm{Mo}} + 20RT\left(\sum_{i=\mathrm{Mo,Ni}} y_i^{\mathrm{II}} \ln y_i^{\mathrm{II}}\right) + {}^{\mathrm{xs}}G_m^{\delta} \quad (4)$$

where ${}^{\circ}G^{\delta}_{\mathrm{Ni}:i:\mathrm{Mo}}$ represents the Gibbs energy of the end-member $(\mathrm{Ni})_{24}(i)_{20}(\mathrm{Mo})_{12}$ with the colon separating components in different sublattices and is given as:

$${}^{\circ}G^{\delta}_{\mathrm{Ni}:i:\mathrm{Mo}} = 24{}^{\circ}G_{\mathrm{Ni}}^{\mathrm{fcc}} + 20{}^{\circ}G_i^{\mathrm{bcc}} + 12{}^{\circ}G_{\mathrm{Mo}}^{\mathrm{bcc}} + \Delta G^{\delta}_{\mathrm{Ni}:i:\mathrm{Mo}} \quad (5)$$

y_i^{II} in Eq. (4) is the site fraction of component i in the second sublattice. ${}^{\circ}G_{\mathrm{Ni}}^{\mathrm{fcc}}$, ${}^{\circ}G_{\mathrm{Mo}}^{\mathrm{bcc}}$, and ${}^{\circ}G_i^{\mathrm{bcc}}$ (i = Ni or Mo) are the Gibbs energies of the pure fcc-Ni, bcc-Mo and bcc-Ni, respectively, from the database by Dinsdale [30]. According to the first-principles data and experimental data [21,22] in Fig. 5, the enthalpy of formation of δ-NiMo is temperature-dependent. The Gibbs energy of formation, $\Delta G^{\delta}_{\mathrm{Ni}:i:\mathrm{Mo}}$, is thus expressed as $a^{\delta}_{\mathrm{Ni}:i:\mathrm{Mo}} + b^{\delta}_{\mathrm{Ni}:i:\mathrm{Mo}}T + c^{\delta}_{\mathrm{Ni}:i:\mathrm{Mo}}T\ln(T)$. ${}^{\mathrm{xs}}G_m^{\delta}$ in Eq. (4) is the excess Gibbs energy, expressed in Redlich–Kister polynomial [32] as

$${}^{\mathrm{xs}}G_m^{\delta} = y_{\mathrm{Ni}}^{\mathrm{II}} y_{\mathrm{Mo}}^{\mathrm{II}} \left(\sum_{k=0} {}^{k}L^{\delta}_{\mathrm{Ni:Ni,Mo:Mo}} (y_{\mathrm{Mo}}^{\mathrm{II}} - y_{\mathrm{Ni}}^{\mathrm{II}})^k\right) \quad (6)$$

where ${}^{k}L^{\delta}$ is the kth interaction parameter, expressed as ${}^{k}a^{\delta} + {}^{k}b^{\delta}T$. $a^{\delta}_{\mathrm{Ni}:i:\mathrm{Mo}}$, $b^{\delta}_{\mathrm{Ni}:i:\mathrm{Mo}}$, $c^{\delta}_{\mathrm{Ni}:i:\mathrm{Mo}}$, ${}^{k}a^{\delta}$, and ${}^{k}b^{\delta}$ are model parameters to be evaluated.

3.3. Ni_3Mo phase

Ni_3Mo has the D0a structure and the space group *pmmn* [18]. The unit cell of Ni_3Mo has eight atoms distributed in three-sublattices, i.e. $Ni_4Ni_2Mo_2$. The experimental data by Heijwegen and Rieck [19] revealed a small composition homogeneity of Ni_3Mo. The non-stoichiometric Ni_3Mo phase is thus described using the three-sublattice model, (Mo, Ni)$_4$(Ni)$_2$(Mo, Ni)$_2$, with the Gibbs energy given as:

$$G_m^{\mathrm{Ni_3Mo}} = \sum_{i=\mathrm{Mo,Ni}} y_i^{\mathrm{I}} \sum_{j=\mathrm{Mo,Ni}} y_j^{\mathrm{III}\circ} G^{\mathrm{Ni_3Mo}}_{i:\mathrm{Ni}:j} + RT \sum_{i=\mathrm{Mo,Ni}} (4y_i^{\mathrm{I}} \ln y_i^{\mathrm{I}} + 2y_i^{\mathrm{III}} \ln y_i^{\mathrm{III}}) + {}^{\mathrm{xs}}G_m^{\mathrm{Ni_3Mo}} \quad (7)$$

Due to the first and third sublattices mainly occupied by Ni and Mo, respectively, the reference state bcc was selected for the third sublattice and fcc for the other sublattices. The Gibbs energy of the end-member i:Ni:j in Eq. (7), ${}^{\circ}G^{\mathrm{Ni_3Mo}}_{i:\mathrm{Ni}:j}$, is given as follows:

$${}^{\circ}G^{\mathrm{Ni_3Mo}}_{i:\mathrm{Ni}:j} = 4{}^{\circ}G_i^{\mathrm{fcc}} + 2{}^{\circ}G_{\mathrm{Ni}}^{\mathrm{fcc}} + 2{}^{\circ}G_j^{\mathrm{bcc}} + \Delta G^{\mathrm{Ni_3Mo}}_{i:\mathrm{Ni}:j} \quad (8)$$

where y^{I} and y^{III} are the site fractions in the first and third sublattices, respectively, ${}^{\circ}G_i^{\mathrm{fcc}}$ and ${}^{\circ}G_j^{\mathrm{bcc}}$ (i, j = Mo and Ni) the Gibbs energy of the elements Mo and Ni from the database by Dinsdale [30]. As mentioned in Section 3.2, the enthalpy of formation of δ-NiMo is temperature-dependent. The same behavior is assumed for Ni_3Mo. The Gibbs energy of formation of the end-member i:Ni:j, $\Delta G^{\mathrm{Ni_3Mo}}_{i:\mathrm{Ni}:j}$, is thus expressed as $a^{\mathrm{Ni_3Mo}}_{i:\mathrm{Ni}:j} + b^{\mathrm{Ni_3Mo}}_{i:\mathrm{Ni}:j}T + c^{\mathrm{Ni_3Mo}}_{i:\mathrm{Ni}:j}T\ln(T)$. ${}^{xs}G_m^{Ni_3Mo}$ in Eq. (8) is the excess Gibbs energy, expressed in the Redlich–Kister polynomial [32] as

$${}^{\mathrm{xs}}G_m^{\mathrm{Ni_3Mo}} = y_{\mathrm{Mo}}^{\mathrm{I}} y_{\mathrm{Ni}}^{\mathrm{I}} \sum_{i=\mathrm{Mo,Ni}} y_i^{\mathrm{III}} \sum_{k=0} {}^{k}L^{\mathrm{Ni_3Mo}}_{\mathrm{Mo,Ni:Ni:}i} (y_{\mathrm{Mo}}^{\mathrm{I}} - y_{\mathrm{Ni}}^{\mathrm{I}})^k + y_{\mathrm{Mo}}^{\mathrm{III}} y_{\mathrm{Ni}}^{\mathrm{III}} \sum_{i=\mathrm{Mo,Ni}} y_i^{\mathrm{I}} \sum_{k=0} {}^{k}L^{\mathrm{Ni_3Mo}}_{i:\mathrm{Ni:Mo,Ni}} (y_{\mathrm{Mo}}^{\mathrm{III}} - y_{\mathrm{Ni}}^{\mathrm{III}})^k \quad (9)$$

where ${}^{k}L^{\mathrm{Ni_3Mo}}$ is the kth interaction parameter, expressed as ${}^{k}a^{\mathrm{Ni_3Mo}} + {}^{k}b^{\mathrm{Ni_3Mo}}T$. $a^{\mathrm{Ni_3Mo}}_{i:\mathrm{Ni}:j}$, $b^{\mathrm{Ni_3Mo}}_{i:\mathrm{Ni}:j}$, $c^{\mathrm{Ni_3Mo}}_{i:\mathrm{Ni}:j}$, ${}^{k}a^{\mathrm{Ni_3Mo}}$, and ${}^{k}b^{\mathrm{Ni_3Mo}}$ are model parameters to be evaluated.

The two-sublattice model was also used in the literature to model the D0a structure [9]. To be compatible with those descriptions, we also develop another set of model parameters with Ni_3Mo being described by the two-sublattice model, i.e. (Mo, Ni)$_3$(Mo, Ni)$_1$, denoted by Ni_3MoII

$$G_m^{\mathrm{Ni_3MoII}} = \sum_{i=\mathrm{Mo,Ni}} y_i^{\mathrm{I}} \sum_{j=\mathrm{Mo,Ni}} y_j^{\mathrm{II}\circ} G^{\mathrm{Ni_3MoII}}_{i:j} + RT \sum_{i=\mathrm{Mo,Ni}} (3y_i^{\mathrm{I}} \ln y_i^{\mathrm{I}} + y_i^{\mathrm{II}} \ln y_i^{\mathrm{II}}) + {}^{\mathrm{xs}}G_m^{\mathrm{Ni_3MoII}} \quad (10)$$

The Gibbs energy of the end-member *i*:*j* in Eq. (10), ${}^{\circ}G^{\mathrm{Ni_3MoII}}_{i:j}$, is given in Eq. (11):

$$ {}^{\circ}G^{\mathrm{Ni_3MoII}}_{i:j} = 3{}^{\circ}G^{\mathrm{ref}}_{i} + {}^{\circ}G^{\mathrm{ref}}_{j} + \Delta G^{\mathrm{Ni_3MoII}}_{i:j} \quad (11) $$

where y^{I} and y^{II} are the site fractions in the first and second sublattices, respectively, ${}^{\circ}G^{\mathrm{ref}}_{i}$ and ${}^{\circ}G^{\mathrm{ref}}_{j}$ (*i*, *j* = Mo and Ni) the Gibbs energy of the elements Mo and Ni in their stable structure at 298 K [30]. The Gibbs energy of formation of the end-member *i*:*j*, $\Delta G^{\mathrm{Ni_3MoII}}_{i:j}$, is expressed as $a^{\mathrm{Ni_3MoII}}_{i:j} + b^{\mathrm{Ni_3MoII}}_{i:j}T + c^{\mathrm{Ni_3MoII}}_{i:j}T\ln(T)$. ${}^{\mathrm{xs}}G^{\mathrm{Ni_3MoII}}_{\mathrm{m}}$ in Eq. (10) is the excess Gibbs energy, expressed in the Redlich–Kister polynomial [32] as

$$ {}^{\mathrm{xs}}G^{\mathrm{Ni_3MoII}}_{\mathrm{m}} = y^{\mathrm{I}}_{\mathrm{Mo}}y^{\mathrm{I}}_{\mathrm{Ni}} \sum_{i=\mathrm{Mo,Ni}} y^{\mathrm{II}}_{\mathrm{i}} \sum_{k=0} {}^{k}L^{\mathrm{Ni_3MoII}}_{\mathrm{Mo,Ni}:i}(y^{\mathrm{I}}_{\mathrm{Mo}} - y^{\mathrm{I}}_{\mathrm{Ni}})^{k} + y^{\mathrm{II}}_{\mathrm{Mo}}y^{\mathrm{II}}_{\mathrm{Ni}} \sum_{i=\mathrm{Mo,Ni}} y^{\mathrm{I}}_{i} \sum_{k=0} {}^{k}L^{\mathrm{Ni_3MoII}}_{i:\mathrm{Mo,Ni}}(y^{\mathrm{II}}_{\mathrm{Mo}} - y^{\mathrm{II}}_{\mathrm{Ni}})^{k} \quad (12) $$

where ${}^{k}L^{\mathrm{Ni_3MoII}}$ is the *k*th interaction parameter, expressed as ${}^{k}a^{\mathrm{Ni_3MoII}} + {}^{k}b^{\mathrm{Ni_3MoII}}T$. $a^{\mathrm{Ni_3MoII}}_{i:j}$, $b^{\mathrm{Ni_3MoII}}_{i:j}$, $c^{\mathrm{Ni_3MoII}}_{i:j}$, ${}^{k}a^{\mathrm{Ni_3MoII}}$, and ${}^{k}b^{\mathrm{Ni_3MoII}}$ are model parameters to be evaluated.

3.4. Ni_2Mo, Ni_4Mo, and Ni_8Mo phases

Ni_2Mo, Ni_4Mo and Ni_8Mo were all treated as stoichiometric compounds. Their Gibbs energy functions are expressed by:

$$ G^{\mathrm{Ni}_i\mathrm{Mo}}_{\mathrm{m}} = a^{\mathrm{Ni}_i\mathrm{Mo}} + b^{\mathrm{Ni}_i\mathrm{Mo}}T + c^{\mathrm{Ni}_i\mathrm{Mo}}T\ln(T) + i{}^{\circ}G^{\mathrm{fcc}}_{\mathrm{Ni}} + {}^{\circ}G^{\mathrm{bcc}}_{\mathrm{Mo}} \quad (13) $$

where $a^{\mathrm{Ni}_i\mathrm{Mo}}$, $b^{\mathrm{Ni}_i\mathrm{Mo}}$, and $c^{\mathrm{Ni}_i\mathrm{Mo}}$ are the model parameters to be evaluated.

4. Model parameter evaluation and result discussion

The model parameters discussed in Section 3 were evaluated using the Parrot module [36] in Thermo-Calc [37], based on the experimental data selected in Section 2. The Parrot module is able to take various types of experimental data simultaneously and minimizes the error of sum with each of the selected data values given a certain weight. The weight is chosen and adjusted based upon the data uncertainties given in the original publications, the intrinsic uncertainties of various experimental techniques, and the modeler's judgment by examining all data concurrently.

The parameter evaluation process started with liquid, followed by bcc and fcc solutions phases and then in the order of δ-NiMo, Ni_3Mo, Ni_4Mo, Ni_2Mo and Ni_8Mo.

The model parameters for the liquid, bcc and fcc phases in Eq. (3) were evaluated with the phase diagram data [17,20], the activity of Mo in fcc [23–26], the Gibbs energy of mixing of fcc [27], and the enthalpy of mixing of bcc and fcc in Table 2 by first-principles calculations. For fcc and bcc, the phase equilibrium data [17–19] and thermochemical data [23–26] were considered as key data and were set to higher weights than the first-principles calculated enthalpies of mixing due to the structure instability and Gibbs energy of mixing of fcc in Ref. [27] due to its too strong temperature-dependent as discussed in Section 2.

Table 3
Thermodynamic properties of the Ni–Mo system per mole of the formula unit

Phase (model)	Parameters	Value
Liquid(Mo, Ni)	${}^{0}L^{\mathrm{liq}}_{\mathrm{Mo,Ni}}$	$-39597 + 15.935T$
	${}^{1}L^{\mathrm{liq}}_{\mathrm{Mo,Ni}}$	$-7373 + 4.102T$
	${}^{2}L^{\mathrm{liq}}_{\mathrm{Mo,Ni}}$	$-12123 + 5.551T$
bcc(Mo, Ni)	${}^{0}L^{\mathrm{bcc}}_{\mathrm{Mo,Ni}}$	27691
	${}^{1}L^{\mathrm{bcc}}_{\mathrm{Mo,Ni}}$	18792
fcc(Mo, Ni)	${}^{0}L^{\mathrm{fcc}}_{\mathrm{Mo,Ni}}$	$-8916 + 3.591T$
	${}^{1}L^{\mathrm{fcc}}_{\mathrm{Mo,Ni}}$	$5469 - 0.249T$
	${}^{2}L^{\mathrm{fcc}}_{\mathrm{Mo,Ni}}$	$-1549 - 2.741T$
δ-NiMo $(Ni)_{24}$ $(Ni, Mo)_{20}(Mo)_{12}$	$\Delta G^{\delta}_{\mathrm{Ni:Mo:Mo}}$	$-169981 + 1154.981T - 155.484T\ln(T)$
	$\Delta G^{\delta}_{\mathrm{Ni:Ni:Mo}}$	$-154106 + 2855.001T - 394.923T\ln(T)$
	${}^{0}L^{\delta}_{\mathrm{Ni:Mo,Ni:Mo}}$	$-829211 + 825.923T$
	${}^{1}L^{\delta}_{\mathrm{Ni:Mo,Ni:Mo}}$	$-417368 + 326.504T$
Ni_2Mo (Ni_2Mo)	$\Delta G^{\mathrm{Ni_2Mo}}_{\mathrm{Ni:Mo}}$	$-28263 + 148.653T - 18.693T\ln(T)$
Ni_3Mo $(Mo, Ni)_4(Ni)_2$ (Mo, Ni)	$\Delta G^{\mathrm{Ni_3Mo}}_{\mathrm{Mo:Ni:Mo}}$	136480
	$\Delta G^{\mathrm{Ni_3Mo}}_{\mathrm{Ni:Ni:Mo}}$	$-81055.2 + 465.054T - 58.929T\ln(T)$
	$\Delta G^{\mathrm{Ni_3Mo}}_{\mathrm{Ni:Ni:Ni}}$	22720
	${}^{0}L^{\mathrm{Ni_3Mo}}_{\mathrm{Mo,Ni:Ni:Mo}}$	−69324
Ni_3MoII(Mo, Ni)$_3$ (Mo, Ni)$_1$	$\Delta G^{\mathrm{Ni_3MoII}}_{\mathrm{Mo:Mo}}$	170600
	$\Delta G^{\mathrm{Ni_3MoII}}_{\mathrm{Ni:Mo}}$	$\Delta G^{\mathrm{Ni_3Mo}}_{\mathrm{Mo:Ni:Ni}}/2$
	$\Delta G^{\mathrm{Ni_3MoII}}_{\mathrm{Mo:Ni}}$	$\Delta G^{\mathrm{Ni_3Mo}}_{\mathrm{Mo:Ni:Mo}}/2$
	$\Delta G^{\mathrm{Ni_3MoII}}_{\mathrm{Ni:Ni}}$	$\Delta G^{\mathrm{Ni_3Mo}}_{\mathrm{Ni:Ni:Ni}}/2$
	${}^{0}L^{\mathrm{Ni_3MoII}}_{\mathrm{Mo,Ni:Mo}}$	−26840
	${}^{0}L^{\mathrm{Ni_3MoII}}_{\mathrm{Ni:Mo,Ni}}$	$4792 - 1.604T$
Ni_4Mo(Ni_4Mo)	$\Delta G^{\mathrm{Ni_4Mo}}_{\mathrm{Ni:Mo}}$	$-45105 + 275.020T - 35.400T\ln(T)$
Ni_8Mo(Ni_8Mo)	$\Delta G^{\mathrm{Ni_8Mo}}_{\mathrm{Ni:Mo}}$	$-55035 + 299.322T - 36.765T\ln(T)$

The model parameters for δ-NiMo are $a^{\delta}_{\mathrm{Ni}:i:\mathrm{Mo}}$, $b^{\delta}_{\mathrm{Ni}:i:\mathrm{Mo}}$, $c^{\delta}_{\mathrm{Ni}:i:\mathrm{Mo}}$, ${}^{k}a^{\delta}$, and ${}^{k}b^{\delta}$ in Eqs. (4)–(6) with *i* representing either Mo or Ni. The parameters $a^{\delta}_{\mathrm{Ni}:i:\mathrm{Mo}}$ were fixed by the first-principles calculation data [13]. The parameters of the end-member $(Ni)_{24}(Mo)_{20}(Mo)_{12}$, $b^{\delta}_{\mathrm{Ni:Mo:Mo}}$ and $c^{\delta}_{\mathrm{Ni:Mo:Mo}}$, were determined using the bcc + δ-NiMo + liquid three-phase equilibrium data [17], the bcc + δ-NiMo two-phase equilibrium data [19], and the enthalpy of formation [21,22]. The parameters of the end-member $(Ni)_{24}(Ni)_{20}(Mo)_{12}$, $b^{\delta}_{\mathrm{Ni:Ni:Mo}}$ and

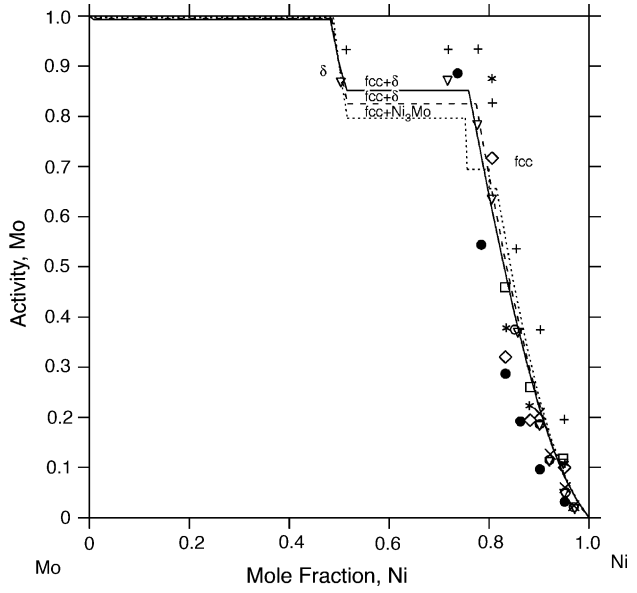

Fig. 6. The calculated activity of Mo in fcc, Ni_4Mo, Ni_3Mo, δ-NiMo and bcc at 1150 K (···), 1273K (- - -) and 1373K (—) with the experimental data at 1373 K (+) and 1273 K (▽) [23]; 1273 K (◯) and 1123 K (×) [24]; 1150 K (□), 1250 K (*), and 1550 K (◊) [25]; 1150 K (●) [26]. Reference state: fcc-Ni and bcc-Mo.

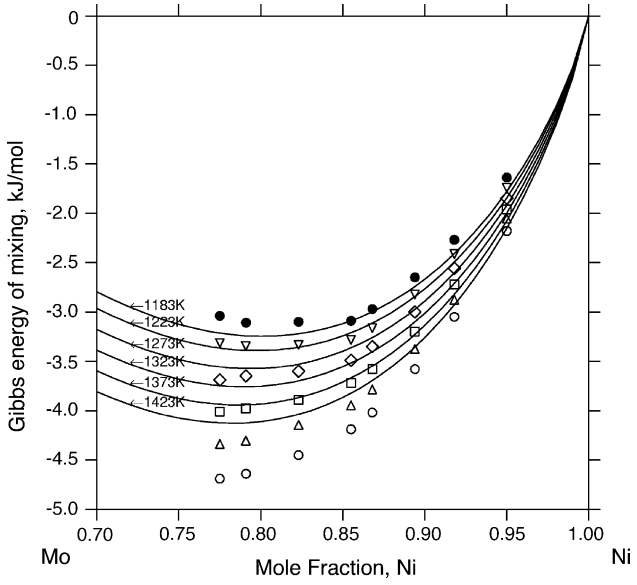

Fig. 7. The calculated Gibbs energy of mixing of fcc at different temperatures with the experimental data (●) at 1183; (▽) at 1233 K; (◊) at 1273 K; (□) at 1323; (△) at 1373 K; (◯) at 1423 K [27]. Reference state: fcc-Ni and bcc-Mo.

$c^{\delta}_{Ni:Ni:Mo}$, were determined through the fcc + δ-NiMo + liquid three-phase equilibrium data [17], the fcc + δ-NiMo two-phase equilibrium data [19], the activity of Mo in fcc and δ-NiMo [23–25], and the enthalpy of formation [21,22]. The interaction parameters, ${}^0a^{\delta}$, ${}^0b^{\delta}$, ${}^1a^{\delta}$, and ${}^1b^{\delta}$ were determined using the first-principles data at the configurations of $Ni_{24}(Mo_{20})Mo_{12}$, $Ni_{24}(Ni_4, Mo_{16})Mo_{12}$, $Ni_{24}(Ni_{16}, Mo_4)Mo_{12}$ and $Ni_{24}(Ni_{20})Mo_{12}$ in Table 2, the phase equilibrium data [17,18], and the experimental enthalpy of formation [21,22].

For Ni_3Mo, the parameters $a^{Ni_3Mo}_{i:Ni:j}$ in the three-sublattice model and $a^{Ni_3MoII}_{i:j}$ in the two-sublattice model were fixed by the first-principles data. The parameters $b^{Ni_3Mo}_{Ni:Ni:Mo}$ and $c^{Ni_3Mo}_{Ni:Ni:Mo}$, $b^{Ni_3MoII}_{Ni:Mo}$ and $c^{Ni_3MoII}_{Ni:Mo}$ and interaction parameters ${}^0L^{Ni_3Mo}$ were evaluated using the fcc + δ-NiMo + Ni_3Mo three-phase equilibrium data [17], the fcc + Ni_3Mo two-phase boundary data [19].

The parameters a^{Ni_iMo} for Ni_4Mo, Ni_2Mo, and Ni_8Mo were fixed by the first-principles data. The parameters b^{Ni_4Mo} and c^{Ni_4Mo} were evaluated with the fcc + Ni_3Mo + Ni_4Mo three-phase equilibrium data [18] and the fcc phase boundary data [18,19]. For Ni_2Mo, the δ-NiMo + Ni_2Mo + Ni_3Mo three-phase equilibrium temperature was assumed to be 1033–1073 K according to the experimental investigation by Pearson et al. [11] and Heijwegen and Rieck [19]. Due to the limit experimental data, the parameter, c^{Ni_2Mo}, was neglected first. Then the parameter, b^{Ni_2Mo}, could be evaluated with the δ-NiMo + Ni_2Mo + Ni_3Mo three-phase equilibrium temperature. However, this makes Ni_3Mo and Ni_4Mo unstable between temperatures 200 and 1000 K because the enthalpies of formation of Ni_3Mo and Ni_4Mo are considered as temperature-dependent. Thus both parameters, b^{Ni_2Mo} and c^{Ni_2Mo}, have to be considered for Ni_2Mo and were evaluated through the Ni_2Mo + Ni_3Mo + δ-NiMo three-phase equilibrium temperature and the Gibbs energy functions of Ni_3Mo and δ-NiMo. With the obtained parameters and three- and two-sublattice models of Ni_3Mo, the calculated δ-NiMo,

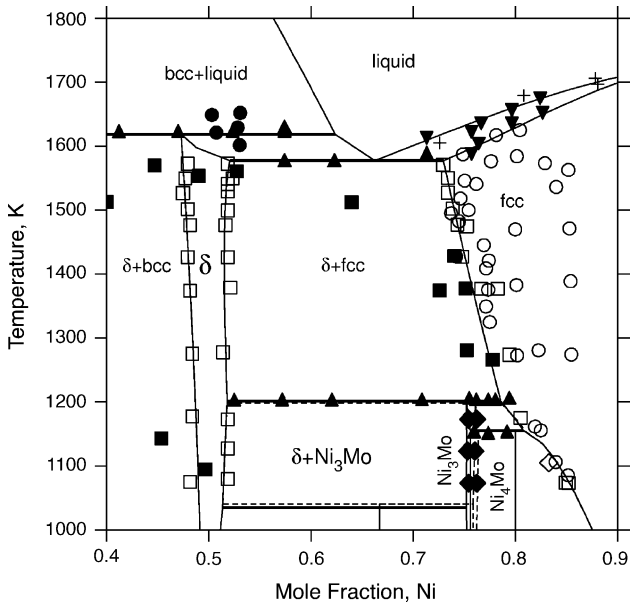

Fig. 8. The calculated phase diagram of the binary Ni–Mo system using the parameters of Ni_3Mo and Ni_3MoII for the solid-lines and dashed-lines, respectively, with the experimental data (▲) three-phase equilibrium, (▼) two-phase field with the liquid phase [17]; (◯) single phase field, (◊) fcc phase boundary, (+, ●) two phase field with liquid phase, (■) two-phase field [18]; (♦) Ni_3Mo phase boundary, (□) phase boundary [19].

Table 4
Invariant reactions of the Ni–Mo system

Reaction	Three-sublattice model's calculated results	Two-sublattice model's calculated results	Experimental results	Ref.
Liquid + bcc → δ-NiMo				
T (K)	1618	1618	1619	[17]
$x_{(liquid,Ni)}$	0.624	0.624	–	
$x_{(bcc,Ni)}$	0.018	0.018	–	
$x_{(\delta,Ni)}$	0.473	0.473	–	
Liquid → δ-NiMo + fcc				
T (K)	1577	1577	1574–1586	[17]
$x_{(liquid,Ni)}$	0.662	0.662	–	
$x_{(\delta,Ni)}$	0.521	0.521	–	
$x_{(fcc,Ni)}$	0.729	0.729	–	
fcc + δ-NiMo → Ni_3Mo				
T (K)	1201	1198	1200	[17]
$x_{(fcc,Ni)}$	0.785	0.786	–	
$x_{(\delta,Ni)}$	0.518	0.518	–	
$x_{(Ni_3Mo,Ni)}$	0.752	0.760	–	
fcc + Ni_3Mo → Ni_4Mo				
T (K)	1151	1150	1148–1150	[17]
$x_{(fcc,Ni)}$	0.808	0.810	–	
$x_{(Ni_3Mo,Ni)}$	0.756	0.764	–	
$x_{(Ni_4Mo,Ni)}$	0.800	0.800	–	
δ-NiMo + Ni_3Mo → Ni_2Mo				
T (K)	1035	1040	1033–1073	[11,19]
$x_{(\delta,Ni)}$	0.513	0.514	–	
$x_{(Ni_3Mo,Ni)}$	0.752	0.758	–	
$x_{(Ni_2Mo,Ni)}$	0.667	0.667	–	
fcc + Ni_4Mo → Ni_8Mo				
T (K)	557	557	555	[12]
$x_{(fcc,Ni)}$	0.980	0.980	–	
$x_{(Ni_4Mo,Ni)}$	0.800	0.800	–	
$x_{(Ni_8Mo,Ni)}$	0.889	0.889	–	
δ-NiMo → bcc + Ni_2Mo				
T (K)	631	631	–	
$x_{(\delta,Ni)}$	0.498	0.498	–	
$x_{(bcc,Ni)}$	0	0	–	
$x_{(Ni_2Mo,Ni)}$	0.667	0.667	–	

Ni_2Mo and Ni_3Mo three-phase equilibrium temperatures are 1035 and 1040 K, respectively. Similar to Ni_2Mo, the parameters, b^{Ni_8Mo} and c^{Ni_8Mo}, were evaluated with its decomposition temperature being 555 K [12] and the Gibbs energy functions of Ni_4Mo and fcc. The parameters, b^{Ni_2Mo} and c^{Ni_2Mo} of Ni_2Mo and b^{Ni_8Mo} and c^{Ni_8Mo}, of Ni_8Mo are desirable to be evaluated with more experimental data in future.

Iterations were needed to evaluate the model parameters when more and more phases were introduced. At the end, all model parameters were allowed to change simultaneously with all selected data included. The final model parameters after truncations are shown in Table 3, and the calculated invariant reactions are listed in Table 4.

With the obtained parameters, the calculated enthalpy of formation at 0 K as a function of composition is shown in Fig. 3 with the first-principles calculation data superimposed [13]. The standard deviation, defined as $\sqrt{\sum_i (A_i - B_i)^2/N}$ to represent the degree of agreement, is 0.68 kJ/mol. The calculated enthalpies of mixing of bcc and fcc are plotted in Fig. 4 together with the first-principles data with the standard deviations of 3.63 and 3.58 kJ/mol for bcc and fcc, respectively. The enthalpy of formation of δ-NiMo with $x_{Ni} = 0.5$ calculated as a function of temperature is shown in Fig. 5 with the standard deviation of 0.51 kJ/mol. The activity data of Mo in fcc, Ni_4Mo, Ni_3Mo, δ-NiMo and bcc [23–26] are shown in Fig. 6 with the standard deviations of 0.14. Fig. 7 shows the calculated Gibbs energy of mixing of fcc with the standard deviation 0.2 kJ/mol from the experimental data [27]. A comparison of the calculated phase diagrams using the three- and two-sublattice models of Ni_3Mo with the experimental data show in the solid lines and dashed-lines in Fig. 8. The complete phase diagram of the Ni–Mo system calculated using the parameters in Table 3 is plotted in Fig. 1. The three-phase equilibrium data [12,17] were compared with the calculated three-phase equilibrium temperature, and the standard deviation is 2.7 K. The rest experimental phase equilibrium data [17–20] were compared with the calculated equilibrium composition with the standard deviation being 0.02.

5. Summary

A new Ni–Mo binary phase diagram was proposed based on first-principles calculations and experimental data. The compounds Ni_2Mo and Ni_8Mo were considered as stable phases, which were not included previously. The δ-NiMo phase stable at high temperature was found not stable at 0 K by the first-principles calculation. The enthalpies of mixing of bcc and fcc were calculated using the SQS's and VASP and used in evaluating model parameters. A self-consistent thermodynamic description of the Ni–Mo binary system is obtained by integrating the first-principles and CALPHAD approaches and serves as part of the thermodynamic database for Ni-base superalloys.

Acknowledgements

This work is supported financially by The Ultra Efficient Engine Technology Program at NASA Glenn Research Center under grant NCC3-920 and the National Science Foundation through the CAREER Award DMR-9983532 and the Information Technology Research Grant DMR-0205232. The Thermo-Calc program is licensed from The Foundation for Computational Thermodynamics and used for all calculations.

References

[1] S. Chakrovorty, D.R.F. West, Mater. Sci. Technol. 1 (1985) 61–72.
[2] E. Aigeltinger, M. Kersker, Met. Forum 4 (1981) 112–116.
[3] B. Grushko, S. Mi, J.G. Highfield, J. Alloys Compd. 334 (2002) 187–191.
[4] R. Jayaram, J.J. Hren, M.K. Miller, Surf. Sci. 246 (1991) 323–328.
[5] R. Jayaram, M.K. Miller, Surf. Sci. 266 (1992) 316–321.
[6] P. Nash, D.T.F. West, Met. Sci. 13 (1979) 670–676.
[7] P. Willemin, M. Durand-Charre, I. Ansara, Liquid–Solid Equilibria in the Systems Ni3Al–Ni3Ta and Ni3Al–Ni3Ti, High Temperature Alloys for Gas Turbines and Other Applications, D Reidel Pub Co., Belgium, 1986.
[8] K. Frisk, CALPHAD 14 (1990) 311–320.
[9] Y. Cui, Z. Jin, X. Lu, Met. Mater. Trans. A 30A (1999) 2735–2744.
[10] M. Morishita, K. Koyama, S. Yagi, G. Zhang, J. Alloys Compd. 314 (2001) 212–218.
[11] D.D. Pearson, B.H. Kear, F.D. Lemkey, in: B. Wilshire, D.R.J. Owen (Eds.), Creep and Fracture of Engineering Materials and Structures, Pineridge, Swansea, 1981.
[12] J. Mayer, K. Urban, Phys. Stat. Sol. (a) 90 (1985) 469–475.
[13] Y. Wang, C. Woodward, S.H. Zhou, Z.K. Liu, L.Q. Chen, Scripta Mater. 52 (2005) 17–20.
[14] J.P. Perdew, J.A. Chevary, S.H. Vosko, K.A. Jackson, M.R. Pederson, D.J. Singh, C. Fiolhais, Phys. Rev. B 46 (1992) 6671–6687.
[15] A. Zunger, S.H. Wei, L.G. Ferreira, J.E. Bernard, Phys. Rev. Lett. 65 (1990) 353–356.
[16] C. Jiang, C. Wolverton, J. Sofo, L.-Q. Chen, Z.K. Liu, Phys. Rev. B 69 (2004) 214202.
[17] G. Grube, H. Schlecht, Z. Elektrochem. 44 (1938) 413–423.
[18] R.E.W. Casselton, W. Hume-Rothery, J. Less-Common Met. 7 (1964) 212–221.
[19] C.P. Heijwegen, G.D. Rieck, Z. Metallkd. 64 (1973) 450–453.
[20] S.J. Kang, Y.D. Song, W.A. Kaysser, H. Hofmann, Z. Metallkd. 75 (1984) 86–91.
[21] P.J. Spencer, F.H. Putland, J. Chem. Thermodyn. 7 (1975) 531–536.
[22] O. Kubaschewski, T. Hoster, Z. Metallkd. 74 (1983) 607–609.
[23] I. Katayama, H. Shimatani, Z. Kozuka, J. Jpn. Inst. Met. 37 (1973) 509–515.
[24] L.L. Meshkov, L.S. Guzei, E.M. Sokolovskaya, Zh. Fiz. Khim. 49 (1975) 1917–1920.
[25] H.L. Tsai, Ph.D. Thesis, University of Tennessee, 1983.
[26] L. Pejryd, Ph.D. Thesis, University of Umea, 1985.
[27] K. Koyama, Y. Hashimoto, K. Suzuki, S. Kameyama, J. Jpn. Inst. Met. 53 (1989) 183–188.
[28] D. Vanderbilt, Phys. Rev. B 41 (1990) 7892–7895.
[29] Y. Wang, S. Curtarolo, C. Jiang, R. Arroyave, T. Wang, G. Ceder, L.-Q. Chen, Z.-K. Liu, CALPHAD 28 (2004) 79–90.
[30] A.T. Dinsdale, CALPHAD 15 (1991) 317–425.
[31] B. Sundman, J. Agren, J. Phys. Chem. Solids 42 (1981) 297–301.
[32] O. Redlich, A.T. Kister, Ind. Eng. Chem. 40 (1948) 345–348.
[33] C.B. Shoemaker, D.P. Shoemaker, Acta Cryst. 16 (1963) 997–1009.
[34] A.V. Virkar, A. Raman, Z. Metallkd. 60 (1969) 594–600.
[35] J.O. Andersson, A.F. Guillermet, M. Hillert, B. Jansson, B. Sundman, Acta Metall. 34 (1986) 437–445.
[36] B. Jansson, Evaluation of Parameters in Thermochemical Models Using Different Types of Experimental Data Simultaneously, TRITA-MAC-0234, Royal Institute of Technology, Stockholm, Sweden, 1984.
[37] J.O. Andersson, T. Helander, L.H. Hoglund, P.F. Shi, B. Sundman, CALPHAD 26 (2002) 273–312.
[38] S.K. Das, G. Thomas, Phys. Stat. Sol. 21 (1974) 177–190.